Title

A novel approach to determine the critical survival threshold of cellular oxygen within spheroids via integrating live/dead cell imaging with oxygen modeling

Authors

Shang, Kuang-Ming
Kato, Hiroyuki
Gonzalez, Nelson
et al.

Publication Date

2024-03-18

DOI

10.1152/ajpcell.00024.2024

METHODS AND RESOURCES

RUNNING HEAD: Determining critical survival pO_2 for islet spheroids

A novel approach to determine the critical survival threshold of cellular oxygen within spheroids via integrating live/dead cell imaging with oxygen modeling

Kuang-Ming Shang[1], Hiroyuki Kato[2], Nelson Gonzalez[2], Fouad Kandeel[2], Yu-Chong Tai[1], Hirotake Komatsu[2]

[1]Department of Medical Engineering, California Institute of Technology, Pasadena, California, United States

[2]Department of Translational Research & Cellular Therapeutics, Arthur Riggs Diabetes & Metabolism Research Institute of City of Hope, Duarte, California, United States

Correspondence: Hirotake Komatsu, MD, PhD (hkomatsu@coh.org)

ABSTRACT

Hypoxia plays a crucial role in cell physiology. Defining the oxygen level that induces cell death within 3D tissues is vital for understanding tissue hypoxia; however, obtaining accurate measurements has been technically challenging. In this study, we introduce a non-invasive, high-throughput methodology to quantify critical survival partial oxygen pressure (pO_2) with high spatial resolution within spheroids by employing a combination of controlled hypoxic conditions, semi-automated live/dead cell imaging, and computational oxygen modeling. The oxygen-permeable, micro-pyramid patterned culture plates created a precisely controlled oxygen condition around the individual spheroid. Live/dead cell imaging provided the geometric information of the live/dead boundary within spheroids. Finally, computational oxygen modeling calculated the pO_2 at the live/dead boundary within spheroids. As proof of concept, we determined the critical survival pO_2 in two types of spheroids: isolated primary pancreatic islets and tumor-derived pseudo-islets (2.43 ± 0.08 vs. 0.84 ± 0.04 mmHg), indicating higher hypoxia tolerance in pseudo-islets due to their tumorigenic origin. We also applied this method for evaluating graft survival in cell transplantations for diabetes therapy, where hypoxia is a critical barrier to successful transplantation outcomes; thus, designing oxygenation strategies is required. Based on the elucidated critical survival pO_2, 100% viability could be maintained in a typically sized primary islet under the tissue pO_2 above 14.5 mmHg. This work presents a valuable tool that is potentially instrumental for fundamental hypoxia research. It offers insights into physiological responses to hypoxia among different cell types and may refine translational research in cell therapies.

NEW & NOTEWORTHY

Our study introduces an innovative combinatory approach for noninvasively determining the critical survival oxygen level of cells within small cell spheroids, which replicates a 3D tissue environment, by seamlessly integrating three pivotal techniques: cell death induction under controlled oxygen conditions, semi-automated imaging that precisely identifies live/dead cells, and computational

modeling of oxygen distribution. Notably, our method ensures high-throughput analysis applicable to various cell types, offering a versatile solution for researchers in diverse fields.

Keywords: Cell survival; Computational simulation; Hypoxia; Pancreatic islets; Viability assay

INTRODUCTION

Hypoxia, characterized by insufficient oxygen availability at the cellular, tissue, or systemic level, plays a pivotal role in both physiological adaptation and pathological processes within the human body. At the molecular level, the response to hypoxia is intricately regulated by the hypoxia-inducible factor 1 alpha (HIF-1α), a key transcription factor that orchestrates downstream molecular functions (1, 2). Hypoxia represents multifaceted adaptive responses that are crucial for survival, with both beneficial and detrimental consequences dictated by the HIF-1α downstream molecular functions. HIF-1α activation triggers essential responses for oxygen delivery including increased erythropoietin to produce red blood cells (3, 4), secretion of vascular endothelial growth factor to facilitate angiogenesis (5), as well as for CD18-mediated inflammation (6). In addition, the duality of hypoxia is evident in its role in normal tissues and cancer cells. Cancer cells exploit hypoxia-inducible factors to thrive in the hostile microenvironment by promoting angiogenesis, metabolic reprogramming, and resistance to cell death (7, 8) which contributes to disease progression.

Although hypoxia is widely acknowledged as a crucial phenomenon in biology and physiology, establishing a universal threshold between normoxia and hypoxia proves challenging. The diversity among cells and tissue types, exemplified by variations between normal and cancer cells, complicates the standardization of cut-off values. Consequently, defining specific critical survival pO_2 values for distinct cell types and tissues is essential, offering insights into their hypoxia resistance in physiological assessments. While theoretically feasible to determine critical survival pO_2 for inducing single-cell death in vitro under precisely controlled hypoxia culture conditions, the ideal scenario involves identifying such thresholds within in vivo-mimicking 3D tissues where physiological cell-cell contact is maintained.

Defining critical survival pO_2 is essential not only for understanding cellular and tissue biology but also for developing cell therapies, particularly evident in pancreatic islet transplantations for patients with type 1 diabetes (9–12). Isolated islet spheroid, a micro-organ consisting of thousands of insulin-secreting cells from the donor pancreas, faces challenges due to the loss of native microvessels during isolation. Relying on interstitial oxygen, cells within the spheroid compete for oxygen, and cells in the spheroid center with increased diffusion distances (average size of 150 μm in diameter) are susceptible to hypoxic stress (13, 14). Thus, islet spheroids are at risk of hypoxia-induced central necrosis, reducing total islet cell mass in culture and transplantation engraftment in islet cell therapy. Several oxygenation approaches have been introduced to prevent hypoxia-induced islet graft loss. Concentrated oxygen was injected into a compartment encasing the transplanted islets (15–17), and co-transplantation techniques incorporating oxygen-containing or oxygen-generating materials improved the viability of transplanted islets (18–20). Although these approaches were experimentally demonstrated to be effective, understanding the critical survival pO_2 of islet cells is crucial for developing improved oxygenation strategies, particularly in estimating exogenous oxygen requirements that ensure the viability of grafts.

While understanding the critical survival pO_2 for cells and tissues is crucial, accurately measuring this pO_2 value within 3D tissues and spheroids presents significant challenges. Direct measurements, such as needle-like Clark electrode (21, 22) and optical fiber methods (23), necessitate the insertion of a sensor tip into the tissues to access the necrotic core; this process intrinsically alters the original oxygen

gradient and, thus, compromises the accuracy of the measurement. Silicone microbeads incorporated into a 3D cell culture and electron paramagnetic resonance imaging (EPR) are potential non-invasive approaches. However, the large size of the beads and the low resolution of EPR are critical barriers to measuring pO_2 in small 3D tissues at the µm level (24–26).

In this study, we present a novel and comprehensive methodology for determining the critical survival pO_2 for 3D cell spheroids; this method integrates three key techniques: 1) inducing cell death within spheroids under precisely regulated oxygen concentrations and geometric parameters (27); 2) employing semi-automated imaging to distinguish live and dead cells within spheroids (28); and 3) utilizing computational modeling to assess oxygen distribution within spheroids (29). Our approach effectively addresses current challenges in defining the critical survival pO_2 within tiny 3D spheroids, offering a non-invasive technique with high spatial resolution data.

MATERIALS AND METHODS

Rat Islet Isolation Procedures

Rat islets were isolated from rat pancreata using our standard procedure (30). Male Lewis rats (Charles River, Wilmington, MA) aged between 16 and 20 weeks and weighing between 400 and 500 grams, were used as islet donors. Under general anesthesia, 9 mL of collagenase solution (2.5 mg/mL, [Sigma-Aldrich, MO], HEPES at 100 mM [Irvine Scientific, Santa Ana, CA] in ice-cold Hanks' balanced salt solution [HBSS; Sigma-Aldrich]) was injected into the pancreatic duct through the common bile duct. The distended pancreas was dissected, followed by enzymatic digestion at 37°C for 10 minutes. The digested pancreas was centrifuged at 300×*g* for 3 minutes. Pellets were washed and subjected to density gradient centrifugation in HBSS solution and Histopaque-1077 (density: 1.077 g/mL, Sigma-Aldrich) for 25 minutes at 300×*g* and 24°C. Islets were hand-picked for purity. The use of animals and animal procedures in this project was approved by City of Hope/Beckman Research Institute Institutional Animal Care and Use Committee. Following isolation, all islets from a single donor were cultured in a 10 cm petri dish (Corning Life Sciences) containing 8 mL of CMRL 1066 culture medium (Corning Life Sciences, Tewksbury, MA) and incubated overnight at 27°C in a CO_2 incubator for recovery. Due to the heterogeneous size of the isolated islets, the standardized unit of Islet Equivalent (IEQ) was used to count the volume-based, normalized islet number, in which the islet with 150 µm in diameter is defined as 1 IEQ (31). Islet yield per donor ranged from 750 to 1200 IEQ, assessed after overnight recovery. Islet purity was assessed before initiating hypoxia experiments and confirmed to be > 90% using our standard procedure with Dithizone staining (iDTZ, Gemini Bio-products, CA) (32).

Production of Pseudo-islets (PsIs)

A rat beta cell line (INS-1 832/13 Rat Insulinoma Cells, Sigma-Aldrich) was used to produce 3D Pseudo-islets (PsIs). After the expansion of the cells in the 2D conventional tissue culture-treated dishes with RPMI1640 medium (Life Technologies, Carlsbad, CA) supplemented with 10% heat-inactivated fetal bovine serum (FBS, Atlanta Biologicals, Lawrenceville, GA), 50 mM of 2-Mercaptoethanol (Sigma-Aldrich), 10 mM of HEPES (Sigma-Aldrich), 1 mM of sodium pyruvate (Sigma-Aldrich), 2 mM of L-glutamine (Sigma-Aldrich), cells were trypsinized into single cells. Dissociated single cells were seeded on a 35 mm-microwell plate (EZSPHERE 900SP; 500 µm-microwell diameters; AGC Techno Glass, Yoshida, Japan) at the seeding density of 1.25×10^6 cells / dish. After the two-day culture of the cells to form the PsIs in a CO_2 incubator at 37°C, PsIs were retrieved for the subsequent experiments. The standardized unit of IEQ was used to count the volume-based, normalized PsIs number (31).

Culture Conditions of Islet Spheroids

One hundred IEQ per well of either isolated rat primary islets or PsIs were seeded onto the micropyramid-patterned, oxygen-permeable bottomed dish (24-well platform) (27), using 1 mL of their specific culture medium described above. The culture dish bottom had the inverse topography of Aggrewell 400 microwell array (Aggrewell 400, STEMCELL Technologies, Vancouver, Canada) made of polydimethylsiloxane (PDMS), which allows for the separation of seeded islets in a uniform oxygen environment throughout the well bottom. The plate was placed within the air-tight modular incubator chambers (Billups-Rothenberg, San Diego, CA), and the designated mixed gas (1% O_2, 5% CO_2, and 94% N_2) was filled using the gas mixer (GB3000, MCQ Instruments, Rome, Italy). The distilled water added to the chamber to provide a humidified culture condition (6.2% $H_2O_{(g)}$). Once the oxygen was reached to the designated partial pressure, the chamber was tightly sealed and placed into the incubator at 37°C. To monitor the partial oxygen pressure within the chamber during the subsequent culture period, the RedEye patch was attached to the inner surface of the modular incubator chamber to non-invasively measure the pO_2 in the chamber from the outside using the optical oxygen sensor (NeoFox, Ocean Optics, Dunedin, FL). The spheroids were cultured for 2 days with no culture medium changes. During the culture period, the pO_2 within the chamber was maintained at the designated value ± 10% deviation (i.e., 0.9 – 1.1% O_2), measured with RedEye patch. At the end of the culture period, the chamber was opened, and the actual pO_2 in the culture medium at the bottom level of the dish, where islets or PsIs were placed, was directly measured by inserting the flexible needle-type optical oxygen sensor (NeoFox, Ocean Optics) that reconfirmed the pO_2 within the 10% deviation to the designated values.

Viability Assessment of Islet Spheroids Using Image Analysis

Viability of islet spheroids (both primary islets and PsIs) was analyzed using live/dead staining by a semi-automated method previously reported (33, 34). Cultured islet spheroids (100 IEQ per group) were incubated in 0.48 µM of fluorescein diacetate (FDA; Sigma-Aldrich) and 15 µM of propidium iodide (PI; Sigma-Aldrich) solution in phosphate-buffered saline for 5 min in the dark at room temperature. Subsequently, they were washed with phosphate-buffered saline and transferred to a 96-well plate to capture the fluorescent images (IX50, Olympus, Tokyo, Japan). By setting thresholds for green (FDA; live cells) and red (PI; dead cells), FDA-positive or PI-positive areas were automatically calculated by the imaging software (cellSens, Olympus). FDA-positive area and PI-positive area were mutually exclusive within the islet spheroids for the analysis (sky blue for FDA-positive areas and magenta for PI-positive areas), and the islet area was defined as the sum of FDA-positive and PI-positive areas. The volumetric viability of an islet sample was calculated as follows: viability (%) = 100 – [(PI-positive area/islet area)^3 × 100]. Shape factor, which numerically describes the shape of a particle under two-dimensional images in a microscope (35) was calculated for all spheroids by the software, and spheroids with shape factor < 0.7 (regarded as non-spherical) were excluded from the analyses. A total of 262 primary islets and 107 PsIs were analyzed.

Oxygen Consumption Rate Measurement

The oxygen consumption rate (OCR) assay was performed for the metabolism assessments of islet spheroids as previously described (36). Approximately 100 IEQ of primary islets or PsIs were plated on a Seahorse XFe islet capture plates (Seahorse Bioscience, North Billerica, MA) and pre-incubated at 37°C in a non-CO_2-incubator for 3 hours. Measurement of the OCR was performed using a Seahorse XFe analyzer (Seahorse Bioscience North Billerica, MA) every 7.5 minutes at 3 mM glucose for 7 measurements. OCR data was normalized by the IEQ applied. OCRs of primary islets from 5 rats and 7 preparations of PsIs were individually measured. The OCR measurement was conducted in an environment with oxygen levels (pO_2) exceeding 120 mmHg to minimize the oxygen gradient between the plastic cell plate and the microchamber containing spheroids. This approach reduced the potential for oxygen diffusion through the plastic cell plate, which could otherwise result in inaccurate OCR

readings. Given that the measurements took place in a well-oxygenated setting, the observed OCR was utilized to estimate the maximal OCR values for the following simulations.

Computational Model of Oxygen Diffusion and Reaction

We employed the finite element method (COMSOL Multiphysics 5.3, MA) to derive the complete pO_2 profile within each islet spheroid and its surrounding microenvironment. The governing equation for oxygen transport, based on Fick's diffusion and reaction, is expressed as:

$$\frac{\partial c}{\partial t} = D\nabla^2 c - R$$

In this equation, c represents the oxygen concentration, D is the oxygen diffusion constant, and R is the oxygen consumption term. The latter follows Michaelis-Menten type metabolic kinetics:

$$R = OCR_{max}\frac{c}{c + K_m}$$

Here, OCR_{max} indicates the maximal oxygen consumption rate, and K_m is the Michaelis constant, corresponding to the oxygen concentration at half the maximum consumption rate. To ensure the continuity of pO_2 across different boundaries, we applied Henry's law to relate the oxygen concentration to pO_2, where S indicated the oxygen solubility:

$$c = S \cdot pO_2$$

Statistical Analysis

Statistical analyses were conducted utilizing the SciPy library (37). Sample sizes were calculated based on the estimated population variance obtained from a preliminary study. This calculation incorporated a z-score of 2.58 to achieve 99% confidence intervals. Data were presented as the mean ± the standard error of the mean (SEM) with relevant percentiles. For the statistical analysis, outliers were excluded if the data points were beyond the 75th percentile plus 1.5 times the interquartile range or below the 25th percentile minus 1.5 times the interquartile range. We employed Pearson's correlation coefficient (r) to quantify the linear relationship between variables. We employed Welch's t-test to address unequal sample sizes and variances. The results reported the *P*-value and an alpha level of 0.01 to interpret the statistical significance.

RESULTS

The method to determine the survival threshold of cellular oxygen within a spheroid was developed by integrating live/dead cell imaging with oxygen modeling.

We employed three techniques: 1) inducing cell death within spheroids under the precisely controlled oxygen and geometric parameters; 2) semi-automated live/dead cell imaging of spheroids; and 3) oxygen computational modeling of spheroids to determine the critical survival pO_2 within spheroids.

We used the air-tight chamber to apply the 1% oxygen at 37°C under atmospheric conditions to induce the initial step—hypoxic cell death within a controlled oxygen microenvironment (Fig. 1A). Subsequently, we seeded spheroids ranging 70–300 µm in diameter at approximately 0.5 spheroids / mm^2 on the micropyramid arrays (which equates to 100 spheroids per well of a 24-well plate) on the oxygen-permeable, micro-pyramid patterned culture plates (27), with 1200 micropyramids per well. This configuration ensured the separation of each islet and prevented the interference of reduced oxygen by the oxygen-consuming neighboring spheroids. Moreover, oxygen-permeable PDMS micropyramids

allowed for 1% oxygen air in the chamber to effectively diffuse from the bottom of the plate to the culture medium around the spheroids. We prepared two representative spheroids, primary rat pancreatic islets and pseudo pancreatic islets (PsIs) derived from a rat beta cell tumor. We cultured them for 2 days, inducing hypoxic cell death in the core of the spheroids. Our culture setup enables investigators to precisely control the pO_2 levels surrounding spheroids and minimize uncertainty and variation in the subsequent computational modeling of the pO_2 profile.

The second step was to acquire the two-color- live/dead fluorescent images of spheroids post 2-day hypoxic culture to extract the parameters required for the subsequent oxygen simulations. Fig. 1B demonstrates the process to extract the radius of the spheroid ($r_{spheroid}$) and dead core (r_{dead}); the pancreatic islet, approximately 150 µm in diameter, consisting of thousands of endocrine cells, is presented. Typically, dead cells are concentrically present in the spheroid's core, which is characteristic of hypoxia-induced central necrosis due to the oxygen gradient within the spheroid. Subsequently, we used a software for semi-automated two-color recognition for live and dead areas to calculate the areas of the spheroid and the dead core. We introduced the concentric model that converts the actual shape traced into a completely circular shape for calculating the estimated radius of the spheroid ($r_{spheroid}$) and the dead core (r_{dead}).

We established a steady state pO_2 profile in the microenvironment within the spheroid by integrating the live/dead imaging parameters in the third step. Fig. 1C illustrates the 3D geometry, boundary conditions, and a cross-sectional pO_2 profile, using a representative spheroid with $r_{spheroid}$ at 73 µm and r_{dead} at 39 µm. We designed the oxygen simulation geometry for the spheroids with the following parameters: each spheroid comprises a concentric inner dead core and an outer live shell; the central necrotic area does not consume oxygen (i.e., $R = 0$); oxygen consumption rate in the outer live shell follows Michaelis-Menten metabolic kinetics; and spheroids were surrounded by culture medium, forming a tall cuboid geometry. We also constructed the oxygen simulation geometry for a micropyramid-shaped, oxygen-permeable PDMS. The height of the medium was 5.3 mm based on a medium volume of 1 mL in a 24-well plate. The cuboid's dimensions, both width and length, were 1.4 mm, which was triple the base side length of the micropyramid. The boundary conditions are established with a 1% oxygen concentration (equivalent to 7.6 mmHg) at both the top and bottom surfaces of the medium. We set the side faces as symmetrical planes under the assumption of negligible oxygen interference between spheroids. A comprehensive list of simulation parameters is presented in Table 1. The OCR data of primary islets and PsIs is available in Supplemental Fig. S1.

The final step was to define the critical survival pO_2 within the spheroid (Fig. 1D). We calculated the critical survival pO_2 by averaging the pO_2 profiles at the boundary between the live shell and the dead core within the spheroid. Collectively, we developed a new method to define the survival threshold of cellular oxygen within a spheroid by integrating the three key techniques.

The method defined the critical survival threshold of cellular oxygen within pancreatic endocrine spheroids.

We applied our newly developed approach to determine the critical survival pO_2 in two types of spheroids for the proof of concept of this approach. We tested 1) primary pancreatic islets isolated from the native pancreas and 2) pseudo-islets derived from the insulin-secreting endocrine cell line. These spheroids secrete insulin; thus, when transplanted as beta cell replacement therapy, they can treat diabetes (38, 39). However, spheroids are vulnerable to hypoxia, which has been one of the roadblocks

to their wide-use beta cell replacement therapy; thousands of oxygen-consuming cells within the spheroids create a steep oxygen gradient and subsequent hypoxia-induced central necrosis. Our new method will determine the physiological oxygen sensitivity of these spheroids by defining the critical survival pO_2 of the cells within the spheroids.

We cultured these spheroids in hypoxia culture at 1% oxygen for 2 days. Fig. 2A demonstrates the representative live/dead stain images of primary islets at pre- and post-culture timepoints in the typical size at r = ~75 µm. We converted the post-culture image into the concentric model image to measure the $r_{spheroid}$, r_{dead}, and viability. Integrating cell imaging data with oxygen modeling identified the critical survival pO_2 of the primary islets at 2.39 mmHg (Fig. 2B). Similarly, Fig. 2C demonstrates the representative live/dead stain images of PsIs with the measured $r_{spheroid}$, r_{dead}, and viability data. The critical survival pO_2 of this specific PsIs was 0.89 mmHg (Fig. 2D). Subsequently, we collected the data of $r_{spheroid}$, r_{dead}, viability, and critical survival pO_2 from individual spheroids of 262 primary islets and 107 PsIs. Live/dead images in various sizes of spheroids (r = 50, 75, and 100 µm) at pre- and post-hypoxic culture are available in Supplemental Fig. S2A (primary islets) and S2B (PsIs). Distribution of the spheroid size in primary islets and PsIs are presented in Supplemental Fig. S2C and S2D. Fig. 2E displays all data plots of $r_{spheroid}$ and r_{dead} in primary islets and PsIs, demonstrating the positive linear correlations between $r_{spheroid}$ and r_{dead}. Overall viability of primary islets and PsIs on day 2 were 75.8 ± 1.1 % and 78.2 ± 1.1 %, respectively (Fig. 2F, P = 0.116). The viability of all individual spheroids is available in Supplemental Fig. S2E (primary islets) and S2F (PsIs).

Lastly, we determined the critical survival pO_2 of individual spheroids and plotted all data according to the spheroid size ($r_{spheroid}$, Fig. 2G). The average critical survival pO_2 values of primary islets and PsIs were 2.43 ± 0.08 mmHg and 0.84 ± 0.04 mmHg, respectively (Fig. 2H); the median and interquartile range (IQR) value of critical survival pO_2 values of primary islets and PsIs were 2.24 (IQR 1.52 – 3.24) mmHg and 0.84 (IQR 0.56 – 1.12) mmHg, respectively. The critical survival pO_2 was lower in PsIs than in primary islets, indicating greater hypoxia resistance in PsIs (P < 0.001). PsIs are derived from beta cell malignant tumor cell line, and malignant cells typically exhibit more hypoxia resistance than the primary non-malignant cells (7, 8). Interestingly, the Fig. 2G showed the negative correlation between the critical survival pO_2 and the radius of spheroids for both primary islets and PsIs (r = -0.15 (P = 0.010) for primary islets; r = -0.33 (P = 0.005) for PsIs). A similar correlation between the critical survival pO_2 and the volume of spheroids ($v_{spheriod}$) for both primary islets and PsIs is also demonstrated in Supplemental Fig. 3 (r = -0.08 (P = 0.174) for primary islets; r = -0.33 (P = 0.005) for PsIs). This may suggest that larger spheroids could provide a more favorable microenvironment at the individual cell level due to a more interconnected organoid structure, despite becoming more vulnerable to hypoxia at the whole spheroid level. Collectively, our novel method not only calculated critical survival pO_2 values of different spheroid types but also elucidated physiological characteristics of the cells and spheroids including the differences in physiological hypoxia resistance of primary vs. malignant cell spheroids.

The critical survival pO_2 contributes to the prediction of the islet graft viability in various oxygen environment.

As demonstrated, elucidating the hypoxia resistance with the critical survival pO_2 values has significance in characterizing the distinct cells. Another potential application using this approach is predicting spheroid survival in various oxygen conditions; this insight is particularly valuable in cell transplantations, including pancreatic islets. Since the hypoxia of the graft site is one of the leading

causes of reducing graft survival in islet transplantations, several oxygenation strategies to improve the transplanted islet graft have been developed (40–44). The critical survival pO_2 values enabled us to accurately simulate graft viability under various oxygen conditions. With the peri-spheroidal pO_2 defined as the oxygen on the surface of the spheroid (Fig. 3A), we employed simulations of the spheroid viability (Fig. 3B). The simulation data estimated the viability for primary islets and PsIs, according to the peri-spheroidal pO_2 and spheroid size ($r_{spheroid}$). This approach provides critical information for designing the oxygenation strategy. For instance, transplant site environment at 5 mmHg (peri-spheroidal pO_2) for a typical-sized rat primary islet with a $r_{spheroid}$ of 75 μm calculates the estimated viability at 70% with the critical survival pO_2 value at 2.43 mmHg. Conversely, to achieve 100% viability for the rat islet, a peri-spheroidal environment of $pO_2 > 15$ mmHg is required.

DISCUSSION

In this study, we introduced an innovative method for determining critical survival pO_2 within islet spheroids. Integrating imaging techniques with computational simulations of 3D spheroids, we identified the pO_2 at live/dead cell boundary with high spatial resolution to define the critical survival pO_2. Cells remain viable above this threshold while they succumb to death below it. Utilizing this model, we uncovered the oxygen sensitivity of pancreatic islet spheroids during acute phases. Importantly, the values identified a difference in physiological characteristics of critical survival pO_2 between primary islets and tumor-derived islet spheroids, confirming higher hypoxia resistance in tumor cells compared to primary cells. Non-malignant primary cells predominantly rely on oxidative phosphorylation for energy production in the presence of oxygen; in contrast, tumor cells generally display aerobic glycolysis for energy production, known as the Warburg effect, contributing to their hypoxia resistance (45). The critical survival pO_2 accurately reflects such physiological processes, underlining the significance of our method in the physiological characterization of cells within spheroids.

Our study demonstrated another potential application of the critical survival pO_2 value for improving cell transplantation outcomes. The hypoxic environment limits the success of pancreatic islet transplantations due to their oxygen-diffusion-limiting spheroidal structure. Correlations among three critical factors in islet transplantations—namely, islet spheroid size ($r_{spheroid}$), surrounding oxygen microenvironment (peri-spheroidal pO_2), and viability of the spheroids—can be determined when the critical survival pO_2 of the spheroids is defined. Calculating the essential peri-transplantation oxygen levels to achieve a desired graft survival rate is a key aspect in developing cell transplantation strategies. In addition to the simple examples in the Results section, it is particularly important when encapsulation techniques are employed to protect islet graft from host immunity (46–49). Macro- and micro-encapsulation, coating islet spheroids with hydrogels or microporous membranes, have shown promise in allogeneic or xenogeneic islet transplantations. Although effective with respect to immunoisolation, oxygen supply for their survival should be carefully considered because the additional layer of hydrogel could restrict oxygen diffusion to the grafts. Understanding the critical survival pO_2 value of the graft cells could provide the estimated graft viability depending on the dimensions and properties of encapsulation materials and devices. In scenarios of severe oxygen deprivation, such as when a large number of islets are encapsulated within a confined space (16), designing the oxygenation strategies is especially important in which the critical survival pO_2 value will serve as a key element to estimate the viability of transplanted cells under varying oxygen conditions.

While previous studies demonstrated methods to determine the critical survival pO_2 value of the cells, critical survival pO_2 values of various cell types and tissues have not been well established. The spearheading work demonstrated the critical survival pO_2 value of the rat-isolated hepatocyte cells at 0.1 mmHg (50). A second study introduced technical advancement by utilizing a fine-tuned, feedback-controlled oxystat system, maintaining steady-state pO_2 between 0.01 mmHg and 150 mmHg in the culture setting (51) but relied on conventional trypan blue staining for single cell viability. The critical survival pO_2 value obtained from these studies was applied to islet cells for the oxygen simulation models (29); however, the approximation deviated from the actual threshold of islet cells, as the values could be cell-type-specific, as demonstrated by others (52), as well as our current study. Advantages of the previous approach include the straightforward methods applicable to any cell type. However, the critical survival pO_2 value of the cell could be only measured in single cells, which could be a crucial limitation for several reasons: the critical survival pO_2 value is likely different in the single cell state vs. actual tissue environment with cell-cell interactions, and the manipulation of the tissue dissociation into single cells itself would damage cells to reduce viability (50). Our method enables the calculation of the pO_2 within the cell spheroids, which mimics the 3D tissue environment. Furthermore, our approach has the following advantageous features: broad applicability across various cell types using non-cell-type-specific viability assessment by live/dead staining, high throughput analytic capability for large quantities of cells, and indirect measurement or the maintenance of a low oxygen tension environment, which eliminates the technical challenges of direct measurements that are prone to drift and susceptible to inaccuracies.

Some limitations in our approach are as follows: First, it does not provide cell type-specific critical survival pO_2 values, particularly when the spheroids are composed of multiple cell types. For example, the primary islets consist of predominantly insulin-secreting beta cells but contain multiple endocrine cells and other cell types. Second, the model operates under the assumption that hypoxia is the primary factor influencing cell survival in the short term within hours – days (13, 50). Multiple molecules, including nutrients, create concentration gradients and contribute to cell death in the longer observation period. Therefore, the method may not be accurate in defining critical survival pO_2 in chronic hypoxic conditions. Third, our method does not define the oxygen threshold of cell function. The cell function may be reduced in the oxygen condition above the critical survival pO_2; therefore, our approach requires other methods, especially for functional analyses. Fourth, the biological variation and fluctuations in the OCR of cells must be carefully considered. For instance, our study utilized primary islets isolated from young male rats. It is well-documented that OCR and insulin-secreting functions vary by sex and age, reflecting mitochondrial functionality (36). Additionally, the OCR is influenced by the microenvironment, such as glucose conditions; high glucose conditions have been shown to increase cell metabolism including OCR (36, 53). Given that OCR is a critical factor in oxygen simulations, employing accurate OCR values and accounting for these variations will contribute to more precise results of the critical survival pO_2. Lastly, we identified a negative correlation between the critical survival pO_2 and spheroid size, which may require thorough interpretation. Our results suggest novel physiological environmental differences between large and small spheroids—the interconnected 3D organoid structure in large spheroids likely creates a favorable microenvironment, despite the occurrence of hypoxia. However, potential technical biases that could influence this size-dependency of the critical survival pO_2 should be carefully considered, although we did not detect such flaws in our methodology.

In summary, we have developed a new method to determine the critical survival pO_2 within 3D cell spheroids, offering a high throughput non-invasive technique with high spatial resolution data.

SUPPLEMENTAL MATERIAL

Supplemental Figs. S1-S3: https://doi.org/10.6084/m9.figshare.24986859

DATA AVAILABILITY

Data are available upon request.

ACKNOWLEDGMENTS

The authors would like to thank Drs. Colin Cook and Nicholas Scianmarello for the insightful discussion. We would also like to thank Dr. Sung Hee Kil for critical reading and editing of the manuscript.

GRANTS

Nora Eccles Treadwell Foundation, No Grant Number (to H. Komatsu);
National Institutes of Health, Grant Number: R03DK129958-01 (to H. Komatsu);
Juvenile Diabetes Research Foundation, Grant Number: 3-SRA-2021-1073-S-B (to H. Komatsu).

DISCLOSURES

No conflicts of interest, financial or otherwise, are declared by the authors.

AUTHOR CONTRIBUTIONS

Conceived and designed research: KMS, HK (Kato), HK (Komatsu);
Performed experiments: KMS, HK (Kato), NG, HK (Komatsu);
Analyzed data: KMS, HK (Kato), HK (Komatsu);
Interpreted results of experiments: KMS, HK (Kato), HK (Komatsu);
Prepared figures: KMS, HK (Kato), HK (Komatsu);
Drafted manuscript: KMS, HK (Komatsu);
Edited and revised manuscript: KMS, HK (Kato), YCT, HK (Komatsu);
Approved final version of manuscript: KMS, HK (Kato), NG, FK, YCT, HK (Komatsu).

REFERENCES

1. **Carmeliet P, Dor Y, Herbert J-M, Fukumura D, Brusselmans K, Dewerchin M, Neeman M, Bono F, Abramovitch R, Maxwell P, Koch CJ, Ratcliffe P, Moons L, Jain RK, Collen D, Keshet E.** Role of HIF-1α in hypoxia-mediated apoptosis, cell proliferation and tumour angiogenesis. *Nature* 394: 485–490, 1998. doi: 10.1038/28867.
2. **Maxwell PH, Wiesener MS, Chang G-W, Clifford SC, Vaux EC, Cockman ME, Wykoff CC, Pugh CW, Maher ER, Ratcliffe PJ.** The tumour suppressor protein VHL targets hypoxia-inducible factors for oxygen-dependent proteolysis. *Nature* 399: 271–275, 1999. doi: 10.1038/20459.
3. **Jelkmann W.** Molecular Biology of Erythropoietin. *Internal Medicine* 43: 649–659, 2004. doi: 10.2169/internalmedicine.43.649.

4. **Bunn HF.** Erythropoietin. *Cold Spring Harb Perspect Med* 3: a011619, 2013. doi: 10.1101/cshperspect.a011619.
5. **Ferrara N.** Vascular Endothelial Growth Factor: Basic Science and Clinical Progress. *Endocrine Reviews* 25: 581–611, 2004. doi: 10.1210/er.2003-0027.
6. **Rosetti F, Mayadas TN.** The many faces of Mac-1 in autoimmune disease. *Immunological Reviews* 269: 175–193, 2016. doi: 10.1111/imr.12373.
7. **Vaupel P, Mayer A, Höckel M.** Tumor Hypoxia and Malignant Progression. In: *Methods in Enzymology*. Academic Press, p. 335–354.
8. **Harris AL.** Hypoxia — a key regulatory factor in tumour growth. *Nat Rev Cancer* 2: 38–47, 2002. doi: 10.1038/nrc704.
9. **Komatsu H, Kandeel F, Mullen Y.** Impact of Oxygen on Pancreatic Islet Survival. *Pancreas* 47: 533, 2018. doi: 10.1097/MPA.0000000000001050.
10. **Stokes RA, Cheng K, Deters N, Lau SM, Hawthorne WJ, O'connell PJ, Stolp J, Grey S, Loudovaris T, Kay TW, Thomas HE, Gonzalez FJ, Gunton JE.** Hypoxia-Inducible Factor-1α (HIF-1α) Potentiates β-Cell Survival after Islet Transplantation of Human and Mouse Islets. *Cell Transplant* 22: 253–266, 2013. doi: 10.3727/096368912X647180.
11. **Garcia-Contreras M, Tamayo-Garcia A, Pappan KL, Michelotti GA, Stabler CL, Ricordi C, Buchwald P.** Metabolomics Study of the Effects of Inflammation, Hypoxia, and High Glucose on Isolated Human Pancreatic Islets. *J Proteome Res* 16: 2294–2306, 2017. doi: 10.1021/acs.jproteome.7b00160.
12. **Gerber PA, Rutter GA.** The Role of Oxidative Stress and Hypoxia in Pancreatic Beta-Cell Dysfunction in Diabetes Mellitus. *Antioxidants & Redox Signaling* 26: 501–518, 2017. doi: 10.1089/ars.2016.6755.
13. **Komatsu H, Cook C, Wang C-H, Medrano L, Lin H, Kandeel F, Tai Y-C, Mullen Y.** Oxygen environment and islet size are the primary limiting factors of isolated pancreatic islet survival. *PLOS ONE* 12: e0183780, 2017. doi: 10.1371/journal.pone.0183780.
14. **Papas KK, De Leon H, Suszynski TM, Johnson RC.** Oxygenation strategies for encapsulated islet and beta cell transplants. *Advanced Drug Delivery Reviews* 139: 139–156, 2019. doi: 10.1016/j.addr.2019.05.002.
15. **Barkai U, Weir GC, Colton CK, Ludwig B, Bornstein SR, Brendel MD, Neufeld T, Bremer C, Leon A, Evron Y, Yavriyants K, Azarov D, Zimermann B, Maimon S, Shabtay N, Balyura M, Rozenshtein T, Vardi P, Bloch K, De Vos P, Rotem A.** Enhanced Oxygen Supply Improves Islet Viability in a New Bioartificial Pancreas. *Cell Transplant* 22: 1463–1476, 2013. doi: 10.3727/096368912X657341.
16. **Ludwig B, Rotem A, Schmid J, Weir GC, Colton CK, Brendel MD, Neufeld T, Block NL, Yavriyants K, Steffen A, Ludwig S, Chavakis T, Reichel A, Azarov D, Zimermann B, Maimon S, Balyura M, Rozenshtein T, Shabtay N, Vardi P, Bloch K, de Vos P, Schally AV, Bornstein SR, Barkai U.** Improvement of islet function in a bioartificial pancreas by enhanced oxygen supply and growth hormone releasing hormone agonist. *Proceedings of the National Academy of Sciences* 109: 5022–5027, 2012. doi: 10.1073/pnas.1201868109.
17. **Ludwig B, Reichel A, Steffen A, Zimerman B, Schally AV, Block NL, Colton CK, Ludwig S, Kersting S, Bonifacio E, Solimena M, Gendler Z, Rotem A, Barkai U, Bornstein SR.** Transplantation of human

islets without immunosuppression. *Proceedings of the National Academy of Sciences* 110: 19054–19058, 2013. doi: 10.1073/pnas.1317561110.

18. **Pedraza E, Coronel MM, Fraker CA, Ricordi C, Stabler CL.** Preventing hypoxia-induced cell death in beta cells and islets via hydrolytically activated, oxygen-generating biomaterials. *Proceedings of the National Academy of Sciences* 109: 4245–4250, 2012. doi: 10.1073/pnas.1113560109.
19. **Wang L-H, Ernst AU, An D, Datta AK, Epel B, Kotecha M, Ma M.** A bioinspired scaffold for rapid oxygenation of cell encapsulation systems. *Nat Commun* 12: 5846, 2021. doi: 10.1038/s41467-021-26126-w.
20. **Oh SH, Ward CL, Atala A, Yoo JJ, Harrison BS.** Oxygen generating scaffolds for enhancing engineered tissue survival. *Biomaterials* 30: 757–762, 2009. doi: 10.1016/j.biomaterials.2008.09.065.
21. **Carlsson PO, Liss P, Andersson A, Jansson L.** Measurements of oxygen tension in native and transplanted rat pancreatic islets. *Diabetes* 47: 1027–1032, 1998. doi: 10.2337/diabetes.47.7.1027.
22. **Murphy KC, Hung BP, Browne-Bourne S, Zhou D, Yeung J, Genetos DC, Leach JK.** Measurement of oxygen tension within mesenchymal stem cell spheroids. *Journal of The Royal Society Interface* 14: 20160851, 2017. doi: 10.1098/rsif.2016.0851.
23. **Quaranta M, Borisov SM, Klimant I.** Indicators for optical oxygen sensors. *Bioanal Rev* 4: 115–157, 2012. doi: 10.1007/s12566-012-0032-y.
24. **Kotecha M, Wang L, Hameed S, Viswakarma N, Ma M, Stabler C, Hoesli CA, Epel B.** In vitro oxygen imaging of acellular and cell-loaded beta cell replacement devices. *Sci Rep* 13: 15641, 2023. doi: 10.1038/s41598-023-42099-w.
25. **Cai Lesher-Pérez S, Kim G-A, Kuo C, M. Leung B, Mong S, Kojima T, Moraes C, D. Thouless M, D. Luker G, Takayama S.** Dispersible oxygen microsensors map oxygen gradients in three-dimensional cell cultures. *Biomaterials Science* 5: 2106–2113, 2017. doi: 10.1039/C7BM00119C.
26. **Kotecha M, Epel B, Ravindran S, Dorcemus D, Nukavarapu S, Halpern H.** Noninvasive Absolute Electron Paramagnetic Resonance Oxygen Imaging for the Assessment of Tissue Graft Oxygenation. *Tissue Engineering Part C: Methods* 24: 14–19, 2018. doi: 10.1089/ten.tec.2017.0236.
27. **Myrick RJ, Shang K-M, Betts JF, Gonzalez N, Rawson J, Izumi K, Koba N, Tsuchiya T, Kato H, Omori K, Kandeel F, Mullen Y, Tai Y-C, Botvinick E, Komatsu H.** Micropyramid-patterned, oxygen-permeable bottomed dish for high density culture of pancreatic islets. *Biofabrication* 15: 015018, 2022. doi: 10.1088/1758-5090/aca79a.
28. **Salgado M, Gonzalez N, Medrano L, Rawson J, Omori K, Qi M, Al-Abdullah I, Kandeel F, Mullen Y, Komatsu H.** Semi-Automated Assessment of Human Islet Viability Predicts Transplantation Outcomes in a Diabetic Mouse Model. *Cell Transplant* 29: 0963689720919444, 2020. doi: 10.1177/0963689720919444.
29. **Buchwald P.** FEM-based oxygen consumption and cell viability models for avascular pancreatic islets. *Theoretical Biology and Medical Modelling* 6: 5, 2009. doi: 10.1186/1742-4682-6-5.
30. **Ito T, Itakura S, Todorov I, Rawson J, Asari S, Shintaku J, Nair I, Ferreri K, Kandeel F, Mullen Y.** Mesenchymal Stem Cell and Islet Co-Transplantation Promotes Graft Revascularization and Function. *Transplantation* 89: 1438, 2010. doi: 10.1097/TP.0b013e3181db09c4.
31. **Ricordi C.** Quantitative and qualitative standards for islet isolation assessment in humans and large mammals. *Pancreas* 6: 242–244, 1991. doi: 10.1097/00006676-199103000-00018.

32. **Komatsu H, Qi M, Gonzalez N, Salgado M, Medrano L, Rawson J, Orr C, Omori K, Isenberg JS, Kandeel F, Mullen Y, Al-Abdullah IH.** A Multiparametric Assessment of Human Islets Predicts Transplant Outcomes in Diabetic Mice. *Cell Transplant* 30: 09636897211052291, 2021. doi: 10.1177/09636897211052291.
33. **Komatsu H, Kang D, Medrano L, Barriga A, Mendez D, Rawson J, Omori K, Ferreri K, Tai Y-C, Kandeel F, Mullen Y.** Isolated human islets require hyperoxia to maintain islet mass, metabolism, and function. *Biochemical and Biophysical Research Communications* 470: 534–538, 2016. doi: 10.1016/j.bbrc.2016.01.110.
34. **Komatsu H, Omori K, Parimi M, Rawson J, Kandeel F, Mullen Y.** Determination of Islet Viability Using a Zinc-Specific Fluorescent Dye and a Semiautomated Assessment Method. *Cell Transplant* 25: 1777–1786, 2016. doi: 10.3727/096368915X689721.
35. **Podczeck F, Newton JM.** A Shape Factor to Characterize The Quality of Spheroids. *Journal of Pharmacy and Pharmacology* 46: 82–85, 1994. doi: 10.1111/j.2042-7158.1994.tb03745.x.
36. **Gonzalez N, Salgado M, Medrano L, Mullen Y, Komatsu H.** Isolated pancreatic islet yield and quality is inversely related to organ donor age in rats. *Experimental Gerontology* 128: 110739, 2019. doi: 10.1016/j.exger.2019.110739.
37. **Virtanen P, Gommers R, Oliphant TE, Haberland M, Reddy T, Cournapeau D, Burovski E, Peterson P, Weckesser W, Bright J, van der Walt SJ, Brett M, Wilson J, Millman KJ, Mayorov N, Nelson ARJ, Jones E, Kern R, Larson E, Carey CJ, Polat İ, Feng Y, Moore EW, VanderPlas J, Laxalde D, Perktold J, Cimrman R, Henriksen I, Quintero EA, Harris CR, Archibald AM, Ribeiro AH, Pedregosa F, van Mulbregt P.** SciPy 1.0: fundamental algorithms for scientific computing in Python. *Nat Methods* 17: 261–272, 2020. doi: 10.1038/s41592-019-0686-2.
38. **Shapiro AMJ, Lakey JRT, Ryan EA, Korbutt GS, Toth E, Warnock GL, Kneteman NM, Rajotte RV.** Islet Transplantation in Seven Patients with Type 1 Diabetes Mellitus Using a Glucocorticoid-Free Immunosuppressive Regimen. *New England Journal of Medicine* 343: 230–238, 2000. doi: 10.1056/NEJM200007273430401.
39. **Ntamo Y, Samodien E, Burger J, Muller N, Muller CJF, Chellan N.** In vitro Characterization of Insulin−Producing β-Cell Spheroids. *Frontiers in Cell and Developmental Biology* 8: 623889, 2021. doi: 10.3389/fcell.2020.623889.
40. **Espes D, Lau J, Quach M, Banerjee U, Palmer AF, Carlsson P-O.** Cotransplantation of Polymerized Hemoglobin Reduces β-Cell Hypoxia and Improves β-Cell Function in Intramuscular Islet Grafts. *Transplantation* 99: 2077, 2015. doi: 10.1097/TP.0000000000000815.
41. **Accolla RP, Liang J-P, Lansberry TR, Miravet IL, Loaisiga M, Sardi BL, Stabler CL.** Engineering Modular, Oxygen-Generating Microbeads for the In Situ Mitigation of Cellular Hypoxia. *Advanced Healthcare Materials* 12: 2300239, 2023. doi: 10.1002/adhm.202300239.
42. **Ludwig B, Rotem A, Schmid J, Weir GC, Colton CK, Brendel MD, Neufeld T, Block NL, Yavriyants K, Steffen A, Ludwig S, Chavakis T, Reichel A, Azarov D, Zimermann B, Maimon S, Balyura M, Rozenshtein T, Shabtay N, Vardi P, Bloch K, de Vos P, Schally AV, Bornstein SR, Barkai U.** Improvement of islet function in a bioartificial pancreas by enhanced oxygen supply and growth hormone releasing hormone agonist. *Proceedings of the National Academy of Sciences* 109: 5022–5027, 2012. doi: 10.1073/pnas.1201868109.
43. **Komatsu H, Rawson J, Barriga A, Gonzalez N, Mendez D, Li J, Omori K, Kandeel F, Mullen Y.** Posttransplant oxygen inhalation improves the outcome of subcutaneous islet transplantation: A

promising clinical alternative to the conventional intrahepatic site. *American Journal of Transplantation* 18: 832–842, 2018. doi: 10.1111/ajt.14497.

44. **Pedraza E, Coronel MM, Fraker CA, Ricordi C, Stabler CL.** Preventing hypoxia-induced cell death in beta cells and islets via hydrolytically activated, oxygen-generating biomaterials. *Proceedings of the National Academy of Sciences* 109: 4245–4250, 2012. doi: 10.1073/pnas.1113560109.
45. **Warburg O.** On the Origin of Cancer Cells. *Science* 123: 309–314, 1956. doi: 10.1126/science.123.3191.309.
46. **Ma M, Chiu A, Sahay G, Doloff JC, Dholakia N, Thakrar R, Cohen J, Vegas A, Chen D, Bratlie KM, Dang T, York RL, Hollister-Lock J, Weir GC, Anderson DG.** Core–Shell Hydrogel Microcapsules for Improved Islets Encapsulation. *Advanced Healthcare Materials* 2: 667–672, 2013. doi: 10.1002/adhm.201200341.
47. **Desai T, Shea LD.** Advances in islet encapsulation technologies. *Nat Rev Drug Discov* 16: 338–350, 2017. doi: 10.1038/nrd.2016.232.
48. **Ernst AU, Wang L-H, Worland SC, Marfil-Garza BA, Wang X, Liu W, Chiu A, Kin T, O'Gorman D, Steinschneider S, Datta AK, Papas KK, James Shapiro AM, Ma M.** A predictive computational platform for optimizing the design of bioartificial pancreas devices. *Nat Commun* 13: 6031, 2022. doi: 10.1038/s41467-022-33760-5.
49. **Kumagai-Braesch M, Jacobson S, Mori H, Jia X, Takahashi T, Wernerson A, Flodström-Tullberg M, Tibell A.** The TheraCyte™ Device Protects against Islet Allograft Rejection in Immunized Hosts. *Cell Transplant* 22: 1137–1146, 2013. doi: 10.3727/096368912X657486.
50. **Anundi I, de Groot H.** Hypoxic liver cell death: critical Po2 and dependence of viability on glycolysis. *American Journal of Physiology-Gastrointestinal and Liver Physiology* 257: G58–G64, 1989. doi: 10.1152/ajpgi.1989.257.1.G58.
51. **Noll T, de Groot H, Wissemann P.** A computer-supported oxystat system maintaining steady-state O2 partial pressures and simultaneously monitoring O2 uptake in biological systems. *Biochemical Journal* 236: 765–769, 1986. doi: 10.1042/bj2360765.
52. **Miranda MA, Macias-Velasco JF, Lawson HA.** Pancreatic β-cell heterogeneity in health and diabetes: classes, sources, and subtypes. *American Journal of Physiology-Endocrinology and Metabolism* 320: E716–E731, 2021. doi: 10.1152/ajpendo.00649.2020.
53. **Kato H, Miwa T, Quijano J, Medrano L, Ortiz J, Desantis A, Omori K, Wada A, Tatsukoshi K, Kandeel F, Mullen Y, Ku HT, Komatsu H.** Microwell culture platform maintains viability and mass of human pancreatic islets. *Frontiers in Endocrinology* 13: 1015063, 2022. doi: 10.3389/fendo.2022.1015063.
54. **Suszynski TM, Avgoustiniatos ES, Papas KK.** Oxygenation of the Intraportally Transplanted Pancreatic Islet. *Journal of Diabetes Research* 2016: e7625947, 2016. doi: 10.1155/2016/7625947.
55. **Xing W, Yin M, Lv Q, Hu Y, Liu C, Zhang J.** 1 - Oxygen Solubility, Diffusion Coefficient, and Solution Viscosity. In: *Rotating Electrode Methods and Oxygen Reduction Electrocatalysts*, edited by Xing W, Yin G, Zhang J. Elsevier, p. 1–31.
56. **Merkel TC, Bondar VI, Nagai K, Freeman BD, Pinnau I.** Gas sorption, diffusion, and permeation in poly(dimethylsiloxane). *Journal of Polymer Science Part B: Polymer Physics* 38: 415–434, 2000. doi: 10.1002/(SICI)1099-0488(20000201)38:3<415::AID-POLB8>3.0.CO;2-Z.

FIGURE LEGENDS

Figure 1. Workflow for determining the critical survival pO_2 in spheroids. *A*: Spheroids are cultured in a controlled hypoxic environment with 1% oxygen (O_2). The structure and material of the culture dish, micropyramid shape and oxygen-permeable PDMS bottom plate, ensure individual islet separation and a uniform oxygen environment for each islet cultured. *B*: An example of the parameter extraction process, which includes post-culture live/dead staining and imaging, semi-automated software-based color recognition of spheroids and dead cores, and conversion into a concentric geometry model to calculate the spheroid radius ($r_{spheroid}$) and dead core radius (r_{dead}). Sky-blue and magenta areas indicate the viable and dead cells, respectively. Scale bar: 100 µm. *C*: A steady-state oxygen diffusion and reaction model for an individual spheroid requires parameters of the spheroid, the micropyramid-bottomed PDMS dish, and the culture medium. Schemas of the three-dimensional geometry (left panel), and the cross-sectional pO_2 profile (right panel) are shown. Scale bar: 200 µm. *D*: Integration of live/dead images (a concentric geometry model, top panel) with oxygen simulations (middle panel) enables calculation of the critical survival pO_2, defined as the pO_2 at the live/dead boundary (bottom panel; a graph demonstrating the pO_2 in the mid-line cross-section of the spheroid). Simulation details and coefficients can be found in Table 1.

Figure 2. The critical survival pO_2 within spheroids. The approach was applied to two types of pancreatic endocrine spheroids: primary pancreatic islets and pseudo-islets (PsIs) derived from the insulin-secreting cell line. *A*: Representative live/dead images of primary islets. A primary islet in the pre-culture (top) and post-culture (bottom), with the extracted parameters demonstrated. Scale bar: 100 µm. *B*: The calculation of the critical survival pO_2, using live/dead images (concentric geometry model, top panel), oxygen simulations (middle panel), and the pO_2 calculation (bottom graph). The data was retrieved from the specific spheroid shown in Fig. 2*A* (post-culture image). Sky-blue and magenta areas indicate the viable and dead cells, respectively. *C*: Representative live/dead images of PsIs. A PsIs in the pre-culture (top) and post-culture (bottom), with the extracted parameters demonstrated. Scale bar: 100 µm. *D*: The calculation of the critical survival pO_2, using live/dead images (concentric geometry model, top panel), oxygen simulations (middle panel), and the pO_2 calculation (bottom graph). The data was retrieved from the specific spheroid shown in Fig. 2*C* (post-culture image). *E*: Scatter plots showing the correlation between $r_{spheroid}$ and r_{dead} in primary islets (left panel, n = 262 spheroids) and in PsIs (right panel, n = 107 spheroids). *F*: Analysis of the overall viability of spheroids. Box plots demonstrate the interquartile range, median, and the data range. Black diamond plots indicate the average. $P = 0.116$ (Welch's t test). *G*: Scatter plots of individual spheroids with the information of $r_{spheroid}$ and critical survival pO_2 in primary islets (left panel) and in PsIs (right panel). *H*: Analysis of the critical survival pO_2 of spheroids. Box plots demonstrate the interquartile range, median, and the data range. Black diamond plots indicate the average. $P < 0.001$ (Welch's t test).

Figure 3. Prediction of the spheroid viability based on the critical survival pO_2 values. *A*: A schema demonstrating the concept. By providing the three values, peri-spheroidal pO_2, radius of spheroid and critical survival pO_2 defined, the viability of the spheroid can be estimated. Sky-blue and magenta areas indicate the viable and dead cells, respectively. *B*: The predicted viability of primary islets. *C*: The predicted viability of pseudo-islets (PsIs).

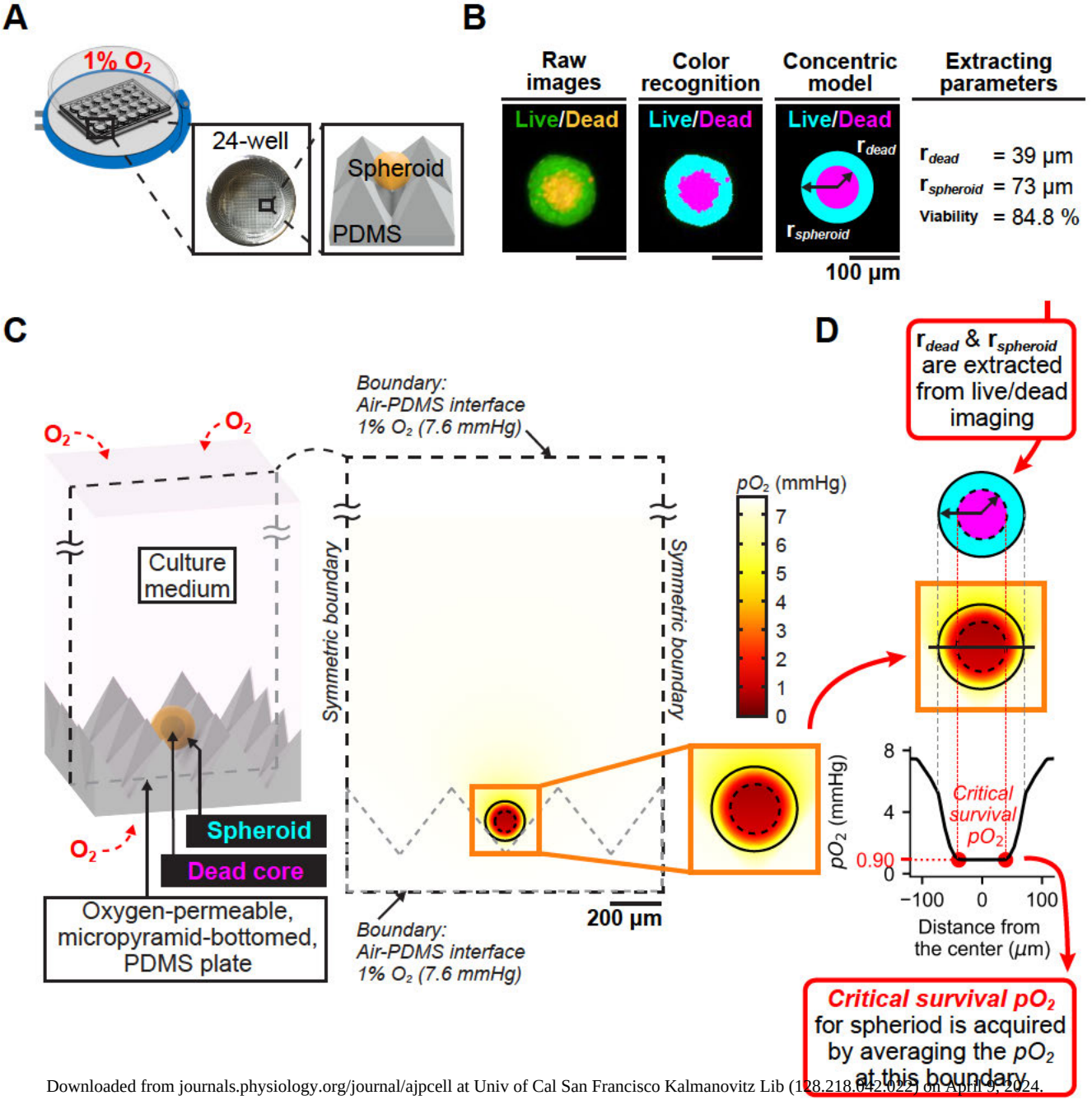

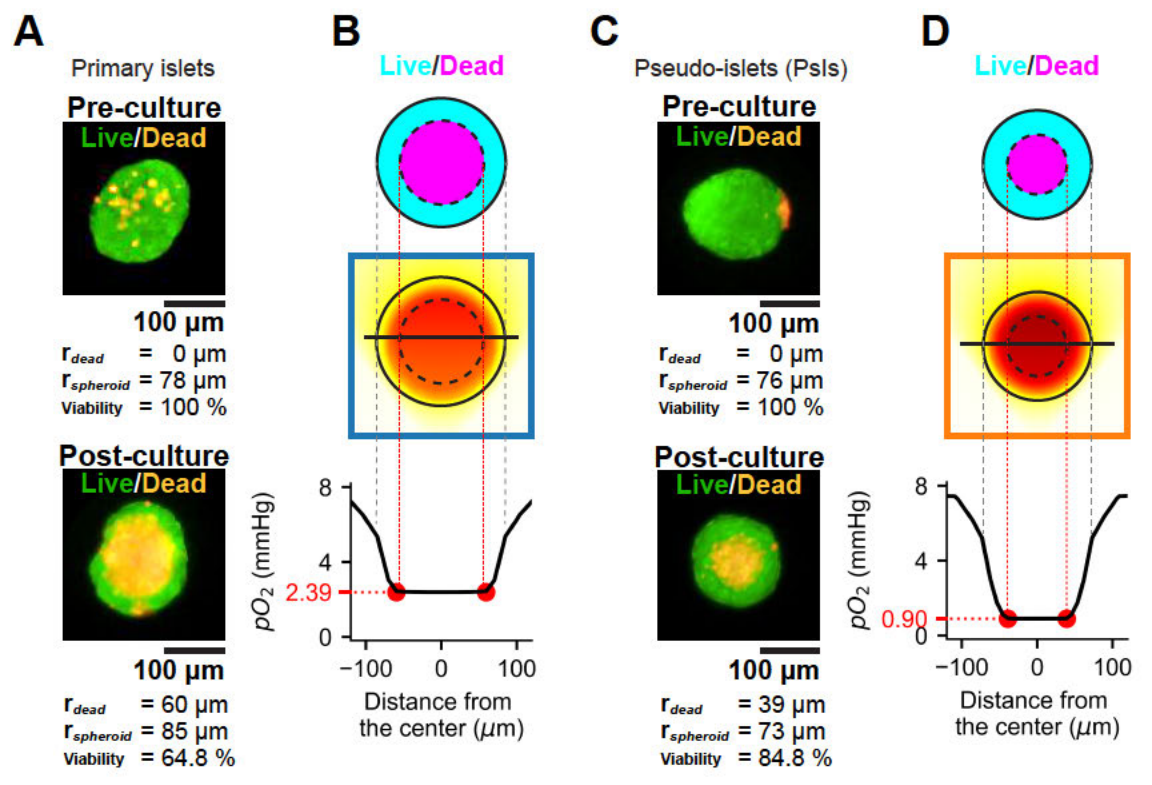

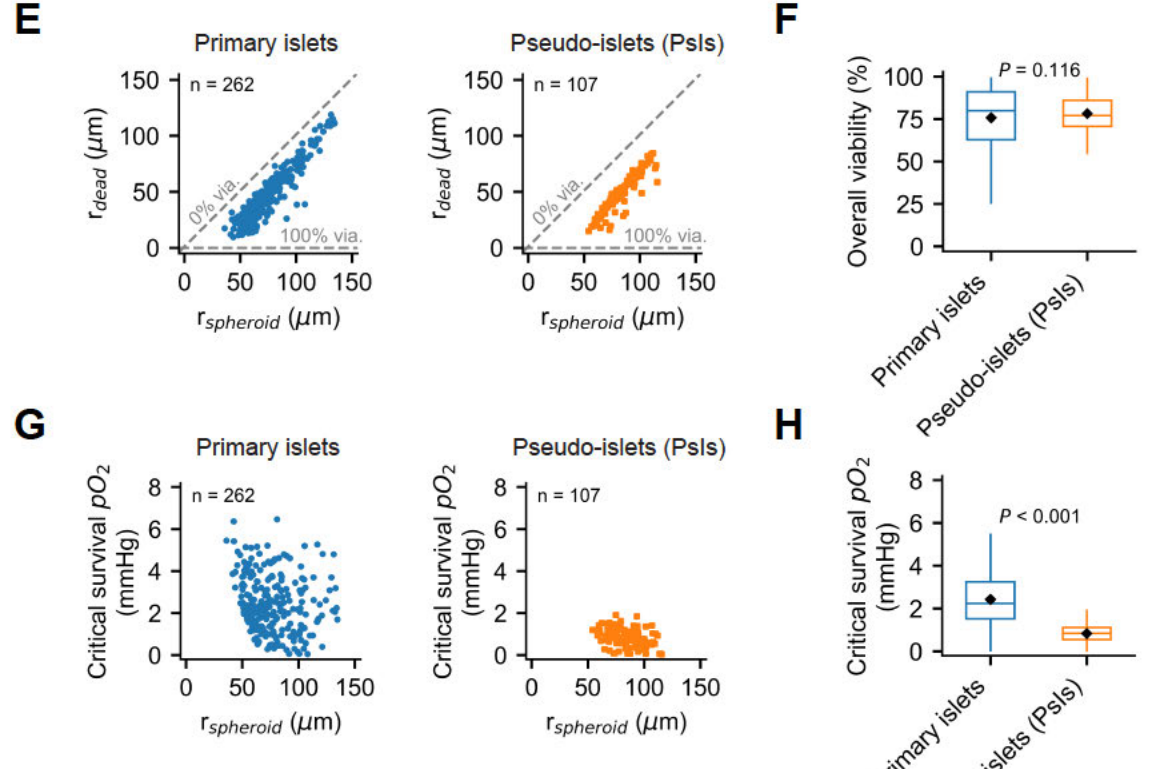

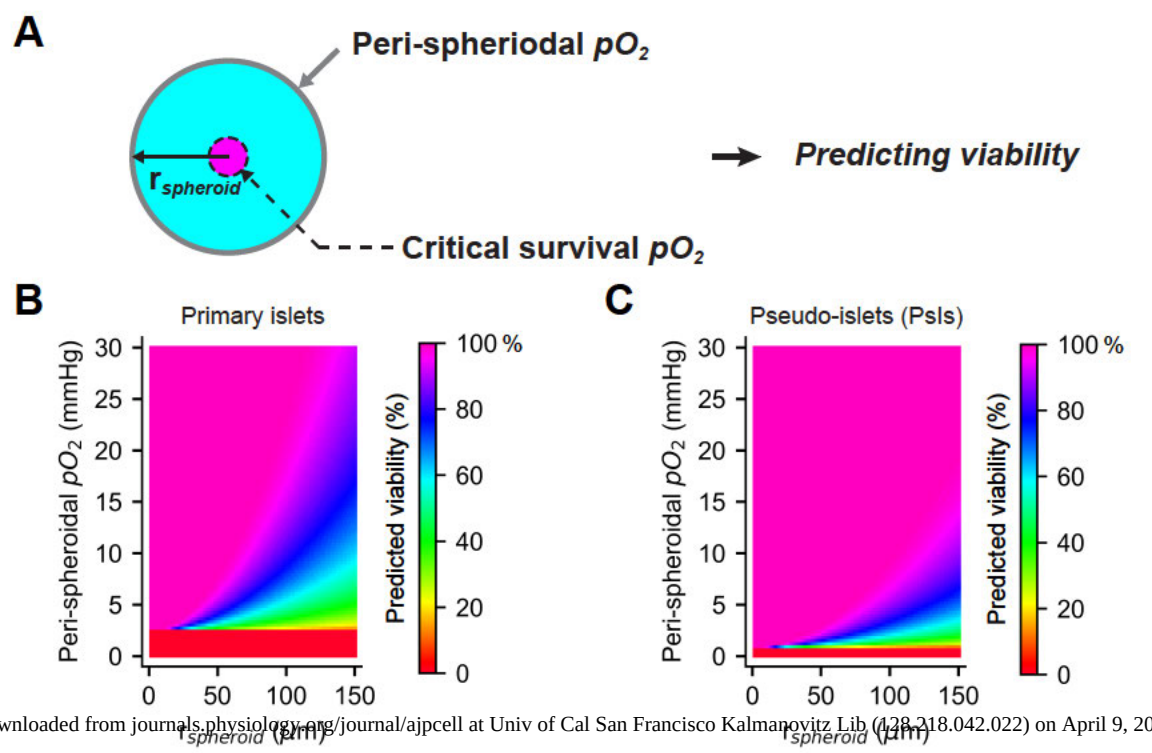

Table 1. Simulation coefficients of oxygen of primary islet, pseudo-islets (PsIs), culture medium, and PDMS.

Materials	**P** (10^{-14} s · mol · kg^{-1})	**D** (10^{-9} m^2 · s^{-1})	**S** (10^{-5} s^2 · mol · kg^{-1} · m^{-2})	$\mathbf{OCR_{max}}$ (mol · m^{-3} · s^{-1})	$\mathbf{K_m}$ (mol · m^{-3})	References
Primary Islets	0.99	1.3	0.76	0.0174*	0.001	(29, 54)
Pseudo-islets (PsIs)	0.99	1.3	0.76	0.0200*	0.001	(29, 54)
Culture Medium	3.05	2.8	1.09	-	-	(10, 55)
PDMS	1.04	7.9	13.2	-	-	(10, 56)

P, Oxygen permeability; **D**, Oxygen diffusivity; **S**, Oxygen solubility coefficient; $\mathbf{OCR_{max}}$, Maximal oxygen consumption rate; $\mathbf{K_m}$, Michaelis oxygen constant; Permeability equals diffusivity times solubility (**P** = **D** × **S**). PDMS denotes polydimethylsiloxane. *Measured in our current study. See also Supplemental Fig. S1.

A Novel Approach to Determine Critical Survival pO_2 for Islet Spheroids

Step 1:
Inducing Hypoxic Cell Death

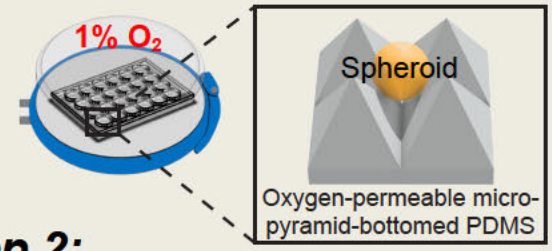

Step 2:
Live/Dead Imaging

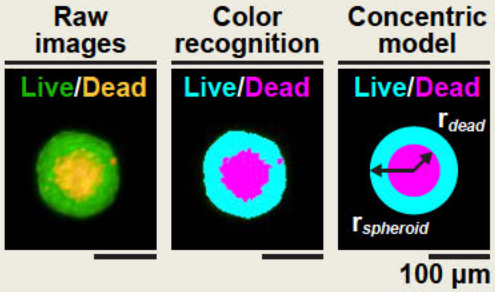

Step 3:
Oxygen Computational Modeling

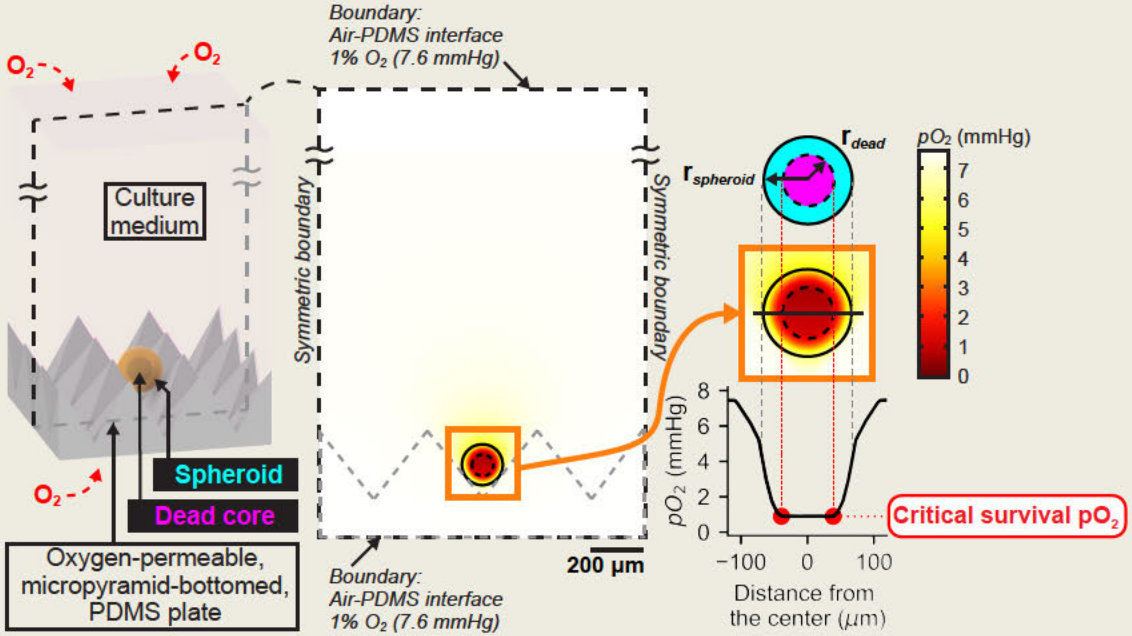

Critical survival pO_2 : **Isolated primary pancreatic islets (2.43 ± 0.08 mmHg)**
Tumor-derived pseudo-islets (0.84 ± 0.04 mmHg)